NASA TECHNICAL MEMORANDUM

NASA TM X-1356

NASA TM X-1356

PERFORMANCE OF A 26-METER-DIAMETER RINGSAIL PARACHUTE IN A SIMULATED MARTIAN ENVIRONMENT

by Charles H. Whitlock, Richard J. Bendura, and Lucille C. Coltrane

Langley Research Center
Langley Station, Hampton, Va.

NATIONAL AERONAUTICS AND SPACE ADMINISTRATION • WASHINGTON, D. C. • MARCH 1967

NASA TM X-1356

PERFORMANCE OF A 26-METER-DIAMETER RINGSAIL PARACHUTE IN A SIMULATED MARTIAN ENVIRONMENT

By Charles H. Whitlock, Richard J. Bendura,
and Lucille C. Coltrane

Langley Research Center
Langley Station, Hampton, Va.

Technical Film Supplement L-946 available on request.

NATIONAL AERONAUTICS AND SPACE ADMINISTRATION

For sale by the Clearinghouse for Federal Scientific and Technical Information
Springfield, Virginia 22151 – CFSTI price $3.00

PERFORMANCE OF A 26-METER-DIAMETER RINGSAIL PARACHUTE IN A SIMULATED MARTIAN ENVIRONMENT

By Charles H. Whitlock, Richard J. Bendura,
and Lucille C. Coltrane
Langley Research Center

SUMMARY

Inflation, drag, and stability characteristics of an 85.3-foot (26-meter) nominal diameter ringsail parachute deployed at a Mach number of 1.15 and at an altitude of 132 600 feet (40.42 kilometers) were obtained from the first flight test of the Planetary Entry Parachute Program. After deployment, the parachute inflated to the reefed condition. However, the canopy was unstable and produced low drag in the reefed condition. Upon disreefing and opening to full inflation, a slight instability in the canopy mouth was observed initially. After a short time, the fluctuations diminished and a stable configuration was attained. Results indicate a loss in drag during the fluctuation period prior to stable inflation. During descent, stability characteristics of the system were such that the average pitch-yaw angle from the local vertical was less than 10^{o}. Rolling motion between the payload and parachute canopy quickly damped to small amplitude.

INTRODUCTION

Parachutes are among the oldest aerodynamic devices used for deceleration. They are presently of interest in deceleration systems for applications such as the NASA Voyager Mars Program. The Langley Research Center has established the Planetary Entry Parachute Program (PEPP) to furnish a technological background to aid in the selection of a deceleration system for the Voyager mission. To meet this objective, flight tests (see ref. 1) which simulate conditions expected in the Martian atmosphere during parachute operation are being conducted. (Altitudes greater than 30 kilometers on earth are required for simulation.) One series consists of carrying a large-size simulated Voyager entry spacecraft to 40 kilometers by balloon. After release from the balloon, rockets accelerate the spacecraft to test conditions and the parachute system is exercised. Onboard camera and accelerometer data are used in conjunction with ground tracking data to evaluate the performance characteristics of the parachute system. The purpose of this paper is to present the basic test results obtained from the first flight of the balloon-launched series of the Planetary Entry Parachute Program. Specifically,

the inflation, drag, and stability data are presented for an 85.3-foot (26-meter) nominal diameter ringsail parachute.

A motion-picture film supplement L-946 is available on loan. The film shows the inflation sequence as taken from an onboard camera.

SYMBOLS

a_l linear acceleration along body longitudinal axis, g units (1g = 9.807 meters per second^2)

$C_{D,o}$ drag coefficient, $\frac{\text{Drag}}{q_\infty S_o}$

$(C_{D,o})_{eff}$ effective drag coefficient, $\frac{2m}{\rho_\infty S_o \dot{Z}_E^2}\left(\ddot{Z}_E - g\right)$

D_o nominal diameter, $\left(\frac{4}{\pi} S_o\right)^{1/2}$, feet (meters)

g acceleration due to gravity, feet per second^2 (meters per second^2)

m mass, $\frac{W}{g}$, slugs (kilograms)

q_∞ free-stream dynamic pressure, pounds per foot^2 (newtons per meter^2)

R Reynolds number

S_o nominal surface area of canopy including all openings such as slots and vent, foot^2 (meter^2)

t time from spacecraft separation, seconds

W weight, pounds (kilograms)

X,Y,Z body axis system

X_E, Y_E, Z_E earth-fixed axis system

ρ_∞ free-stream upper air density, slugs per foot^3 (kilograms per meter^3)

θ, ϕ, ψ payload attitude angles relative to earth-fixed axis system, radians or degrees

δ payload resultant pitch-yaw angle from the local vertical, radians or degrees

Dots over symbols denote differentiation with respect to time. Velocities, dynamic pressures, and Mach numbers are free-stream values unless otherwise noted.

PARACHUTE DESCRIPTION

Characteristics of the fully inflated parachute are given in the following table:

Parachute type	Ringsail
Nominal diameter	85.3 ft (26 m)
Projected diameter	56 ft (17.1 m)
Nominal area	5707 ft^2 (530 m^2)
Projected area	2463 ft^2 (229 m^2)
Canopy material	Dacron
Number of sails (ninth sail omitted)	13
Number of gores	72
Geometric porosity	15 percent
Number of suspension lines	72
Length of suspension lines	78 ft (23.8 m)
Suspension-line material	Dacron
Length of riser lines	6 ft (1.8 m)
Weight	81.1 lb (36.8 kg)
Center of gravity	85.2 ft (26 m)
Pitch and yaw inertia	1820 slug-ft^2 (2466 kg-m^2)
Roll inertia	1220 slug-ft^2 (1653 kg-m^2)

Sketches showing the canopy configuration, and pertinent dimensions for the fully inflated and reefed parachute are presented in figures 1 to 3. Figure 4 shows the principal spacecraft components including various parts of the parachute. Weight, center of gravity, and inertias are for the complete parachute configuration including riser lines, suspension lines, canopy, and so forth. The parachute center-of-gravity position is measured from the payload riser-line attachment location. Inertias are about the parachute center of gravity. Both the inertias and the center-of-gravity position are estimated values based on a rigid system.

The basic ringsail configuration was modified in the following manner. The upper four sails were actually rings separated by slots. The ninth sail (measured from the apex) was omitted to provide 15-percent geometric porosity. The gore dimensions were calculated for a parachute with 76 gores even though it was actually constructed with 72 gores. Some conical shaping of the canopy resulted from this modification.

The parachute was reefed to 16 percent D_o during deployment by a 1500-pound test Dacron line threaded through 72 heavy stainless-steel rings evenly spaced around the mouth of the canopy. The system was disreefed by pryotechnically actuated reefing-line cutters.

SPACECRAFT DESCRIPTION

The principal components of the total spacecraft consisted of an aeroshell, the payload, ballast, and the test parachute. (See fig. 4.) During the thrusting phase of flight, the payload, ballast, and parachute are enclosed in the aeroshell. After parachute deployment, the payload and ballast are extracted from the aeroshell and the ballast is later released; thus, only the parachute and payload comprise the descent system.

Onboard instrumentation consisted of five motion-picture cameras located on the aeroshell and the payload; and normal, transverse, and longitudinal accelerometers located within the payload. Camera 1 had a high frame rate (approximately 500 frames per second) for viewing the inflation process. Cameras 2 and 3 ran at 16 frames per second and were used for determining payload motions from photographs of the horizon and landmarks. The aeroshell cameras (cameras 4 and 5) ran at 64 frames per second and photographed both the parachute inflation process and the payload separation from the aeroshell. Deceleration loads were recorded on a ±50g longitudinal accelerometer. The normal and transverse accelerometers had a range of ±5g.

The payload configuration with ballast attached resembled a 45° frustrum-cylinder with a diameter ratio of 0.384. Length and diameter of the cylinder were approximately 3.24 feet (0.988 meter) and 1.77 feet (0.539 meter), respectively. Mass properties of the suspended payload after parachute deployment are given in the following table:

Property	With ballast	Without ballast
Weight	516 lb (234 kg)	193 lb (88 kg)
Center of gravity	0.5 ft (0.152 m)	1.69 ft (0.515 m)
Pitch inertia	20.2 slug-ft^2 (27.4 kg-m^2)	10.1 slug-ft^2 (13.7 kg-m^2)
Yaw inertia	20.1 slug-ft^2 (27.2 kg-m^2)	9.3 slug-ft^2 (12.6 kg-m^2)
Roll inertia	5.07 slug-ft^2 (6.87 kg-m^2)	2.35 slug-ft^2 (3.18 kg-m^2)

The payload center-of-gravity location is measured rearward from the front of the cylinder or frustrum-cylinder juncture. Parachute bridle attachment points were located radially 0.66 foot (0.20 meter) from the longitudinal axis at a station 3.18 feet (0.97 meter) from the frustrum-cylinder juncture. Spacing about the circumference was equidistant.

TEST ENVIRONMENT

The test described herein was conducted with the use of the balloon launch technique described in reference 1. The mission profile is shown in figure 5. Generally, the sequence of events was as follows. A balloon lifted the spacecraft to an altitude near 40 kilometers. The spacecraft was released (t = 0) by a command signal from the test control center. After separation, the spacecraft fell approximately 4 seconds before the rocket motors ignited and propelled the vehicle to transonic velocities. After burnout, a mortar ejected the parachute (t = 7 seconds) and the deployment sequence was initiated. The parachute was first inflated in a reefed condition, and after a short time period (approximately 4 seconds) the canopy was disreefed to full-inflation diameter. When the parachute drag exceeded the aeroshell drag, the payload was extracted from the rear of the aeroshell, and the parachute-payload combination flew a separate trajectory from the aeroshell. After apogee, a ballast weight was released from the payload at t = 30 seconds in order to obtain reduced descent velocities.

Atmospheric conditions were monitored near the time of flight. From best available data, atmospheric density and pressure variations during flight were assumed to be those shown in figures 6 and 7. Also shown are the 1962 standard atmosphere values. Best available wind velocity and direction data as obtained from an Arcasonde flight 1 hour after launch are shown in figure 8.

The data period for parachute testing began at the time of mortar firing and extended until t = 165 seconds. The trajectory of the parachute-payload combination is shown in figure 9. Altitude and velocity time histories are presented in figure 10; and Mach number and dynamic pressure variations are shown in figure 11. Figure 12 shows the Reynolds number time history.

PARACHUTE PERFORMANCE

The primary objective of the flight test was the determination of inflation, drag, and stability characteristics for the 85.3-foot (26-meter) diameter ringsail parachute. For convenience, each property is considered separately and the results are summarized

in a subsequent section. A motion-picture supplement has been prepared and is available on loan. A request card and a description of the film will be found at the back of this paper.

Inflation Characteristics

The inflation sequence was initiated by a mortar firing the packed parachute rearward from the aeroshell. The parachute bag was open at one end so that first the suspension lines and then the canopy were strung out as the separation distance between the bag and the aeroshell increased. When the bag stripped off the canopy, the parachute inflated to the reefed condition. After approximately 4 seconds, the canopy was disreefed, and the parachute opened to the fully inflated condition. Photographs taken from the aeroshell cameras showing the inflation sequence are presented in figure 13. Figure 13(a) shows inflation to the reefed condition beginning at a time just prior to bag strip. Figure 13(b) shows the canopy configuration fluctuating in the reefed condition. Figure 13(c) presents photographs during disreefing. It appears that reefing line friction may have hindered the opening to fully inflated conditions. Figure 13(d) shows the fully inflated parachute. The noncircular mouth suggests slight canopy instability or breathing prior to 16 seconds. Beyond this time, all data indicate that the canopy assumed a stable configuration. Figure 14 shows photographs of the test taken by a long-range ground camera.

Longitudinal accelerations as obtained by onboard accelerometers are shown in figure 15. Extensive calibration and a zero reference during flight result in an estimated inaccuracy in the accelerometer readings of $\pm 0.2g$. Time is estimated to be accurate within 0.01 second. Also shown are the pertinent events during the inflation phase. The values were obtained by correlation of film and accelerometer records and the event times are estimated to be accurate within 0.1 second. These results indicate that the most severe load during the inflation process was ignition of the explosive separation nut which held the payload and aeroshell together. Between the events of disreefing and aeroshell-payload separation, the loads history is complicated by unknown relative motion between the aeroshell and partially contained payload. From aeroshell-payload separation to the time of stable inflation, severe oscillations are apparent. The exact reason for the accelerometer oscillations has not been determined. Several possible causes are system elasticity, canopy breathing, payload wake interaction, or accelerometer error due to the instruments not being located at the system (parachute and payload) center of gravity. Analysis of the photographs taken from the aeroshell shows a high-frequency oscillation of the payload; this result agrees with the observed accelerometer oscillation. This motion was apparently caused by the aeroshell being at an angle of attack during payload separation.

By means of trigonometric relations, photographs from cameras 4 and 5 were used to estimate the circumference of the canopy mouth during inflation. Figure 16 shows the data obtained and a final extrapolated history based on both camera and accelerometer data. During the period between 10 and 12 seconds, it was difficult to determine precisely the shape of the mouth because of lack of contrast between the canopy interior and cloud background. A first-order error analysis indicates possible inaccuracy of 6 feet in measuring the mouth of the canopy. The primary source of error was the lack of repeatability in tracing the canopy mouth shape from a photograph. The results of figure 16 indicate that parachute disreefing was initiated at approximately 12.6 seconds or 5 seconds after line stretch. As previously discussed, the film data indicate some fluctuation of the canopy mouth between the times of full inflation and stable inflation. Actual data were not obtained in this period because of the large separation distance between the aeroshell and parachute canopy. (See fig. 13(d).)

Drag Characteristics

Drag characteristics for the parachute-payload system were determined by using onboard accelerometer and trajectory data. Drag coefficients for the reefed configuration were estimated from the following equation:

$$C_{D,o} = \frac{-Wa_l - \text{Aeroshell drag}}{q_\infty S_o} \tag{1}$$

The weight of the aeroshell-payload-parachute combination was 1295 pounds (588 kg). Average values of the accelerations between 9.0 (after the opening shock) and 12.5 seconds shown in figure 15 were used. Aeroshell drag was calculated by using the best estimates of aeroshell drag coefficient from unpublished data and free-stream Mach number and dynamic pressure. Figure 17 shows the calculated drag coefficient variation with free-stream Mach number for the reefed configuration and a table for the estimated aeroshell drag coefficient. Also shown is the uncertainty based on a first-order error analysis using 2.8-percent velocity error, 3-percent density error, and 0.3g accelerometer error. The accelerometer error is based on 0.2g instrument error plus 0.1g possible error for using average values. (Use of average values would not be correct if the accelerometer oscillation is caused by off-center-of-gravity instrument location and rotational motion.) Because of the use of free-stream conditions, these drag coefficient results should not be considered applicable to systems which use another configuration as the towing body. Local conditions in the wake of the aeroshell are not presently available.

Drag coefficients for the fully inflated configuration were estimated from the following equation:

$$C_{D,o} = \frac{-Wa_l}{q_\infty S_o} \tag{2}$$

The weight of the system (with apparent and included masses) was assumed as 609 pounds (276 kg). Average accelerations between 14.5 and 23.0 seconds (fig. 15) were used. Accelerometer data beyond this time were not utilized because the results were of questionable validity. Figure 18 presents the calculated $C_{D,o}$ values. The uncertainty in the accelerometer-derived results is based on 15-foot-per-second velocity error, 3-percent density error, and 0.2g instrument error. The total accelerometer error consisted of instrument error plus an error equal to the amplitude of oscillation about the average acceleration values.

In order to verify the results obtained from the onboard accelerations, the flight trajectory was simulated by using the electronic digital process described in reference 2. Previously discussed mass properties and atmospheric conditions were assumed, and tracking data were used to determine initial conditions. Iteration techniques were used to determine the $C_{D,o}$ history which best fitted the flight trajectory between 14.5 and 28.0 seconds. The final curve which produced the best simulation is shown in figure 18. The uncertainty is based on a 15-foot-per-second velocity error and a 3-percent density error in the trajectory being simulated. The simulation results verify the reduced drag between the full-inflation and stable-inflation conditions. At low Mach numbers (corresponding to trajectory apogee), both sets of results contain large uncertainties. The simulation studies indicate that motions and angles of attack near apogee may be large because of wind effects. This condition causes both sets of data in figure 18 to be of questionable value below Mach number 0.25.

Values of the "effective" drag coefficient $C_{D,o}$ based on vertical acceleration and descent velocity were calculated after ballast release (near-vertical descent) by using the following equations:

$$(C_{D,o})_{eff} = \frac{2m}{\rho_\infty S_o \dot{Z}_E^2}(\ddot{Z}_E - g) \tag{3}$$

where $\dot{Z}_E$ and $\ddot{Z}_E$ are the vertical velocity and acceleration (positive downward), respectively. The weight of the parachute-payload system was 275 pounds (125 kg). Figure 19 shows the variation of $(C_{D,o})_{eff}$ with altitude. The uncertainty is based on 3-percent density error, 1.7-percent $\dot{Z}_E$ error, and 12.5-percent $\ddot{Z}_E$ error.

Stability Characteristics

Stability characteristics of the descending parachute system were determined from trajectory and onboard camera data. Photographs from camera 2 (fig. 4) viewing the horizon were analyzed by using the methods of reference 3 extended to the particular

situation of this test. Attitude angles of the payload relative to the local horizon were obtained. The body axis and Euler angle system shown in figure 20 was used for ease of data reduction. The angle ψ is the azimuth of the body X-axis, and its history is an indication of the rolling motion of the system. The angles θ and ϕ are measures of the pitching and yawing motions, and the resultant angle δ is the total pitch-yaw displacement of the longitudinal axis from the local vertical.

Time histories of θ, ϕ, and δ depicting the pitching and yawing motions after ballast release are shown in figure 21. These data are estimated to be accurate within 3°. Data showing the attitude of the parachute relative to the payload were not obtained during the test. Theoretical calculations indicate that pitch-yaw oscillations of the payload relative to the parachute should have a frequency of approximately 0.25 cycle per second. The lack of a significant oscillation in this frequency range suggests that payload pitch-yaw motion relative to the parachute is a minimum. The δ history shows an average or trim angle of less than 10° over most of the data period. The error due to uneven riser line lengths causing an angle between the parachute and payload is estimated to be less than 1°. Figure 22 shows δ as a function of altitude. Initial motions appear to damp until an altitude of 134 000 feet is reached. The divergent motion beginning at this altitude apparently is caused by the wind shear at 135 000 feet. (See fig. 8.) Another wind shear at 129 000 feet causes a reduction in the amplitude of oscillation near 128 000 feet. Below 128 000 feet, the wind shears (fig. 8) cause the erratic motions (fig. 22).

Observation of the film data (payload camera 2) shows relative motion between the parachute and payload about the longitudinal axis. The same result is indicated by the time history of ψ shown in figure 23. Review of the aeroshell camera 5 film indicates that at the time of aeroshell-payload separation, the payload and aeroshell were spinning at a rate of approximately 20° per second in a clockwise direction (looking forward from inertial space). At the same time, the parachute canopy appeared to spin in a counterclockwise direction at a rate near 10° per second. This initial relative motion between the two bodies caused twisting of the shroud and riser lines which apparently set up the roll oscillation. Accurate data could not be obtained until $t = 46$ seconds because of the initial spin rate. The results from this time indicate high roll damping until small amplitudes (less than 5°) are reached. Only moderate damping is apparent for small oscillations. The slowly varying trim value of ψ suggests that the payload is oscillating about the roll axis as the parachute canopy spins slowly in the counterclockwise direction. Small configuration asymmetries in the canopy area would cause such a motion.

CONCLUDING REMARKS

Inflation, drag, and stability characteristics of an 85.3-foot (26-meter) nominal diameter ringsail parachute were obtained from the first flight of the balloon-launched series of the Planetary Entry Parachute Program. After deployment at a Mach number of 1.15, the parachute inflated to the reefed condition. The canopy configuration, however, was not stable and fluctuated rapidly in the reefed condition. The drag coefficient produced during this period was also low. After disreefing and opening to full-inflation conditions, some small fluctuation of the canopy mouth was observed until time 16 second (Mach number, 0.54). Beyond this time, both ground-based and onboard cameras show stable inflation for the remainder of the data period. Results indicate a loss of drag during the period when the canopy mouth was fluctuating prior to stable inflation. Payload attitude data after ballast release show good stability characteristics with an average resultant pitch-yaw amplitude of less than 10° from the local vertical. Rolling motions between the payload and parachute canopy appeared to damp to small amplitude quickly.

Langley Research Center,
National Aeronautics and Space Administration,
Langley Station, Hampton, Va., February 1, 1967,
709-08-00-01-23.

REFERENCES

1. McFall, John C., Jr.; and Murrow, Harold N.: Parachute Testing at Altitudes Between 30 and 90 Kilometers. AIAA Aerodynamic Deceleration Systems Conference, Sept. 1966, pp. 116-121.

2. James, Robert L., Jr. (with appendix B by Norman L. Crabill): A Three-Dimensional Trajectory Simulation Using Six Degrees of Freedom With Arbitrary Wind. NASA TN D-641, 1961.

3. Anon.: Manual of Photogrammetry. Sec. ed., American Soc. of Photogrammetry, c.1952.

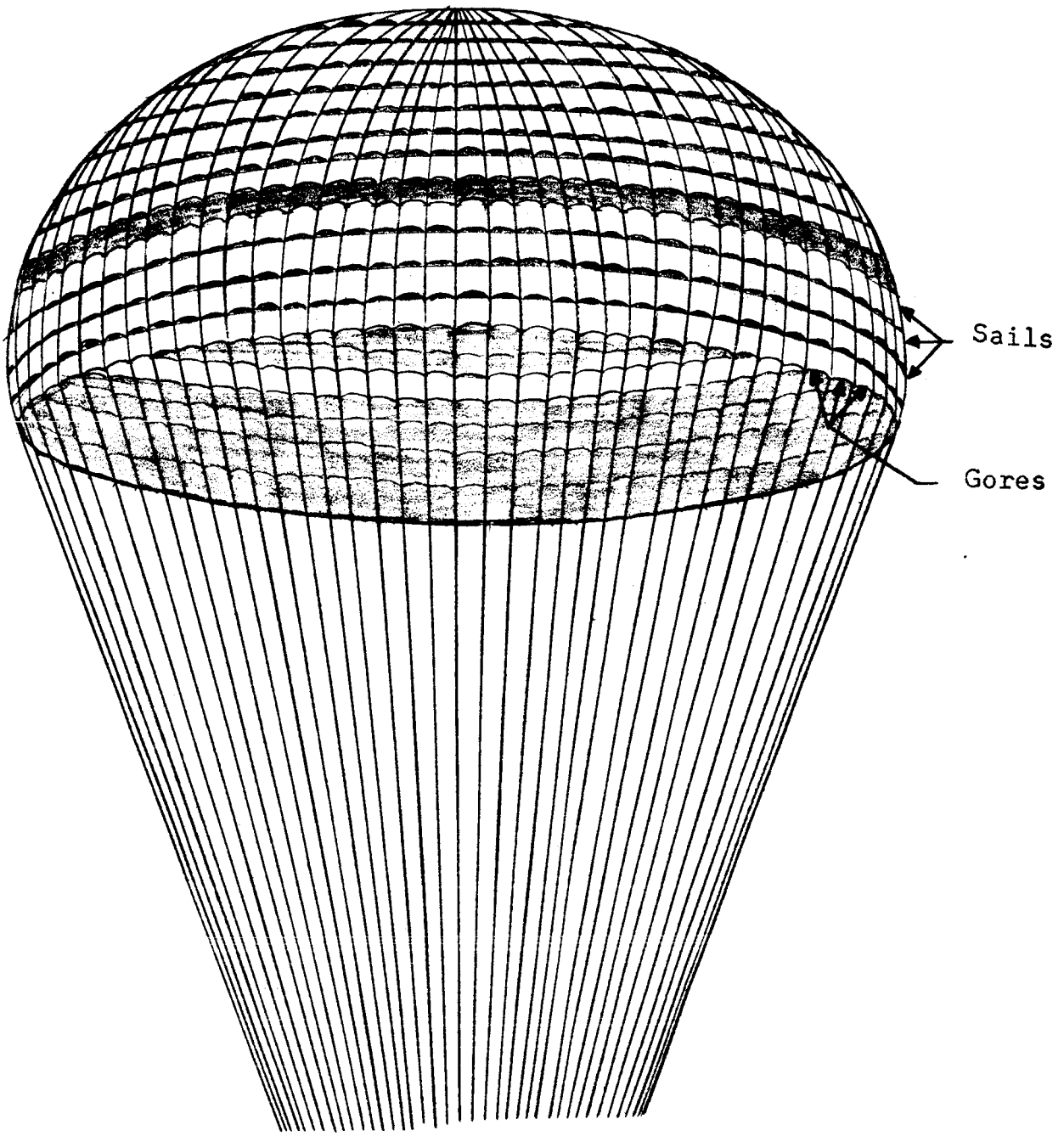

Figure 1.- Ringsail canopy configuration.

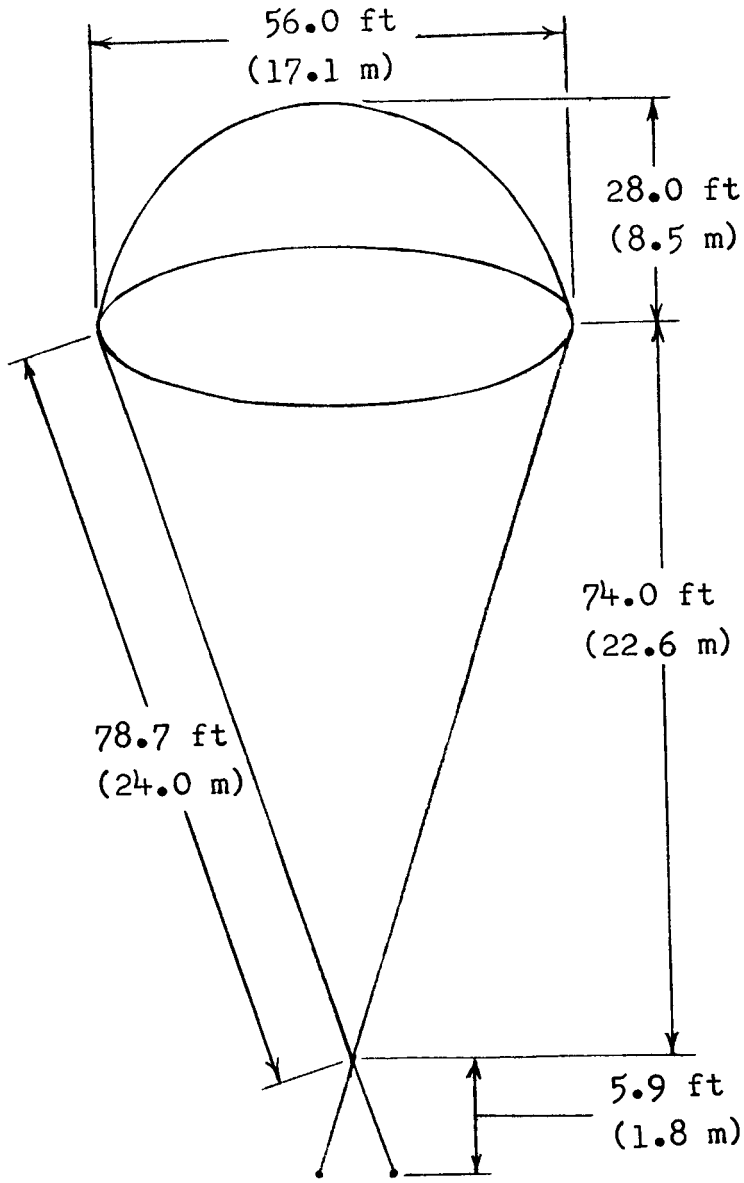

Figure 2.- Sketch of nominal fully inflated parachute. (Dimensions are approximate and sketch is not to scale.)

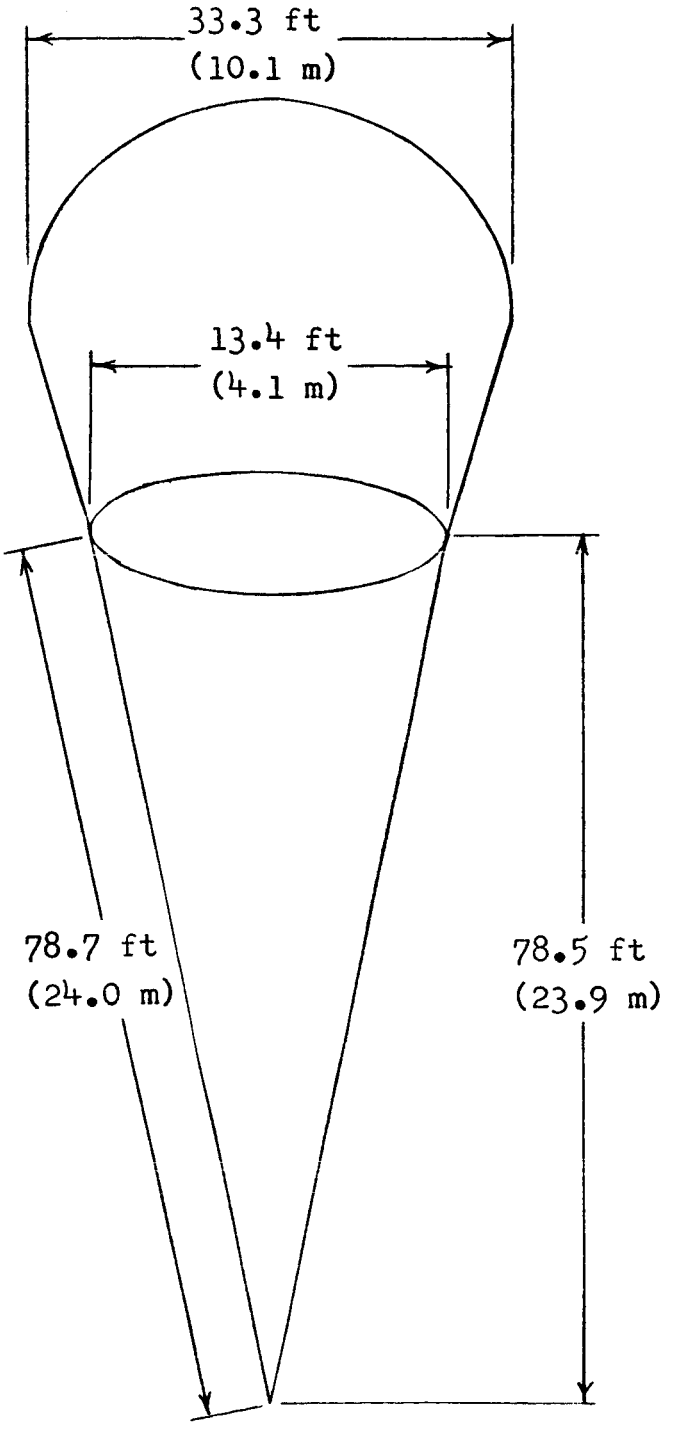

Figure 3.- Sketch of nominal reefed parachute. (Dimensions are approximate and sketch is not to scale.)

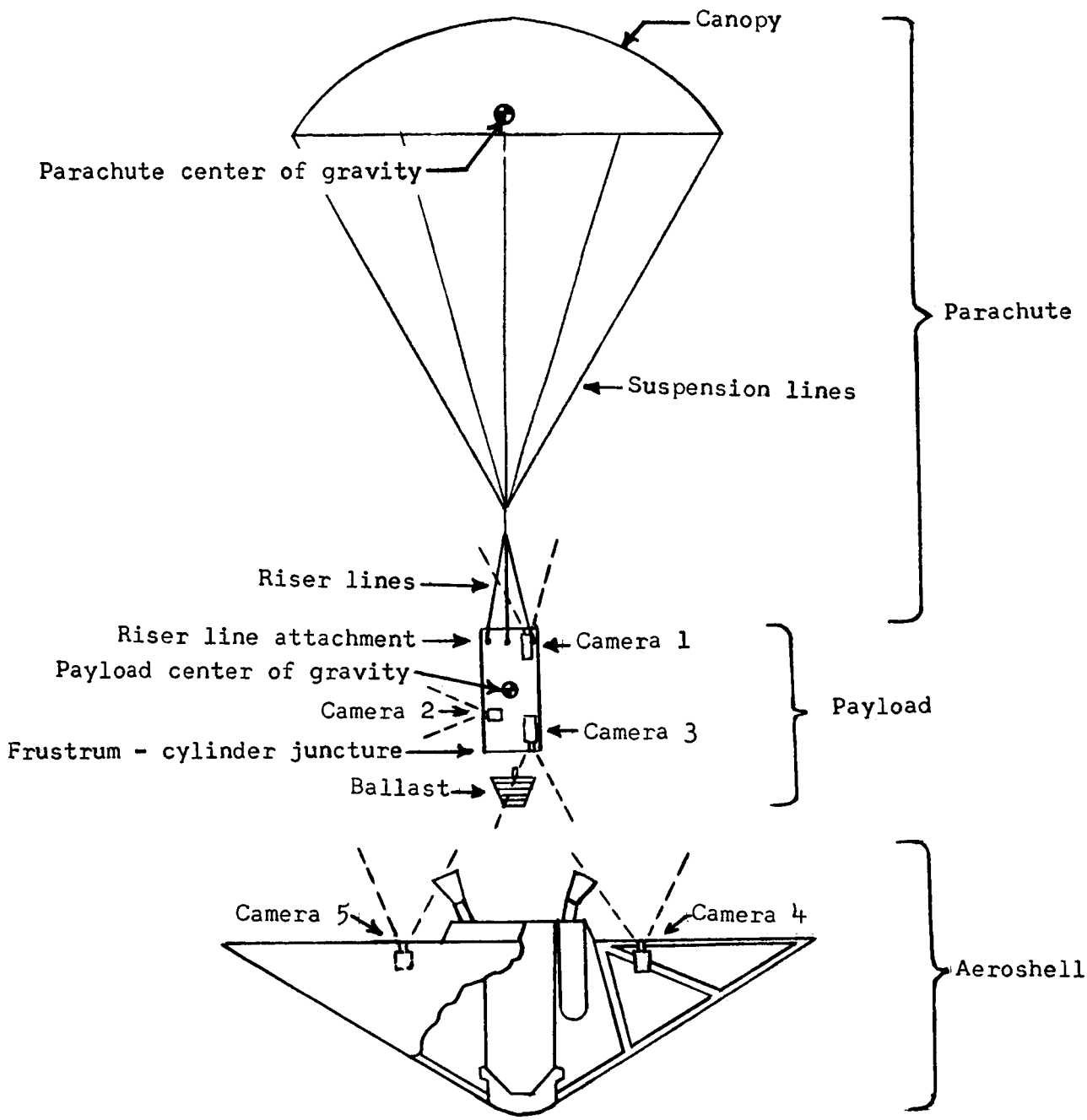

Figure 4.- Sketch of spacecraft components.

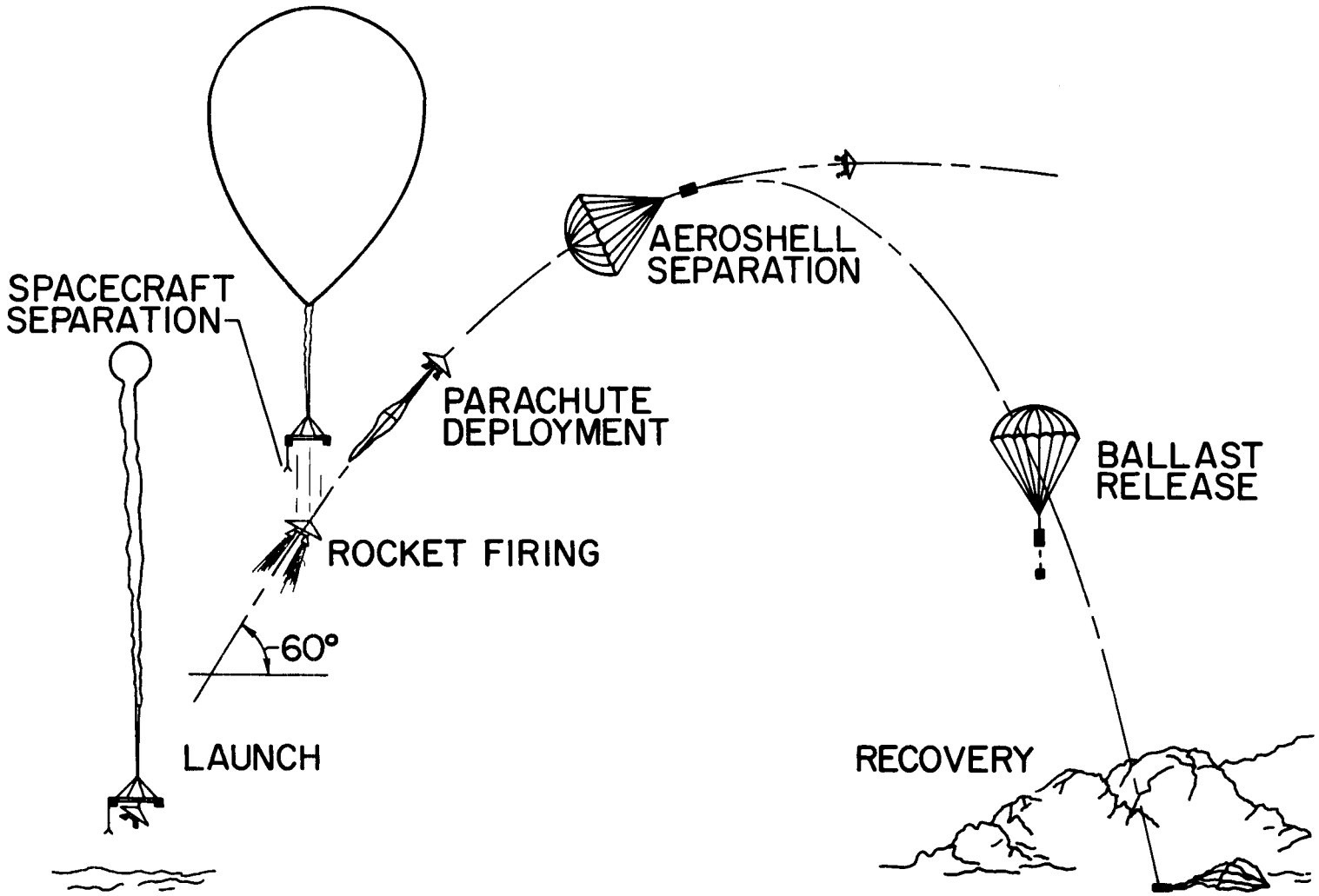

Figure 5.- Mission profile.

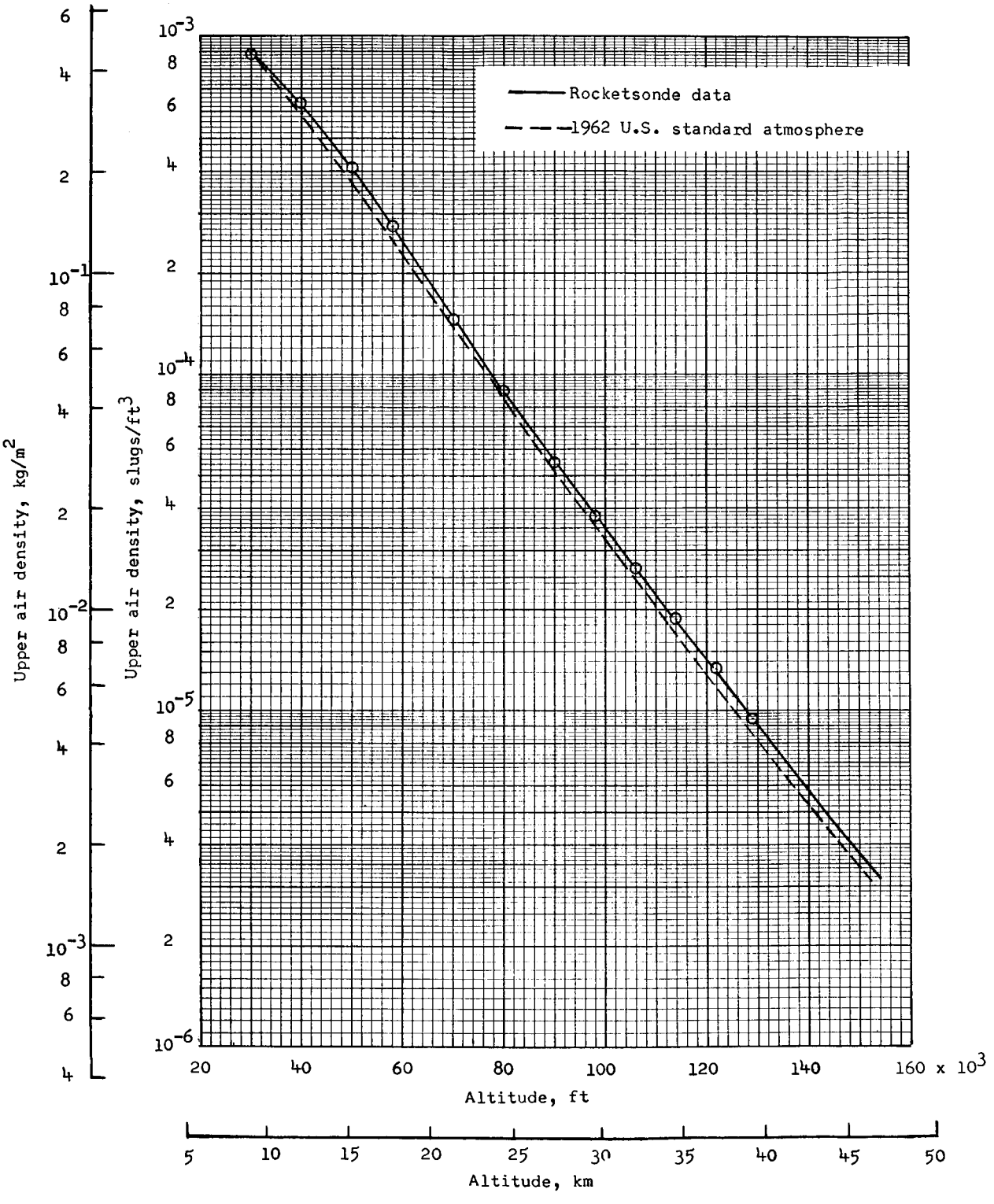

Figure 6.- Atmospheric density.

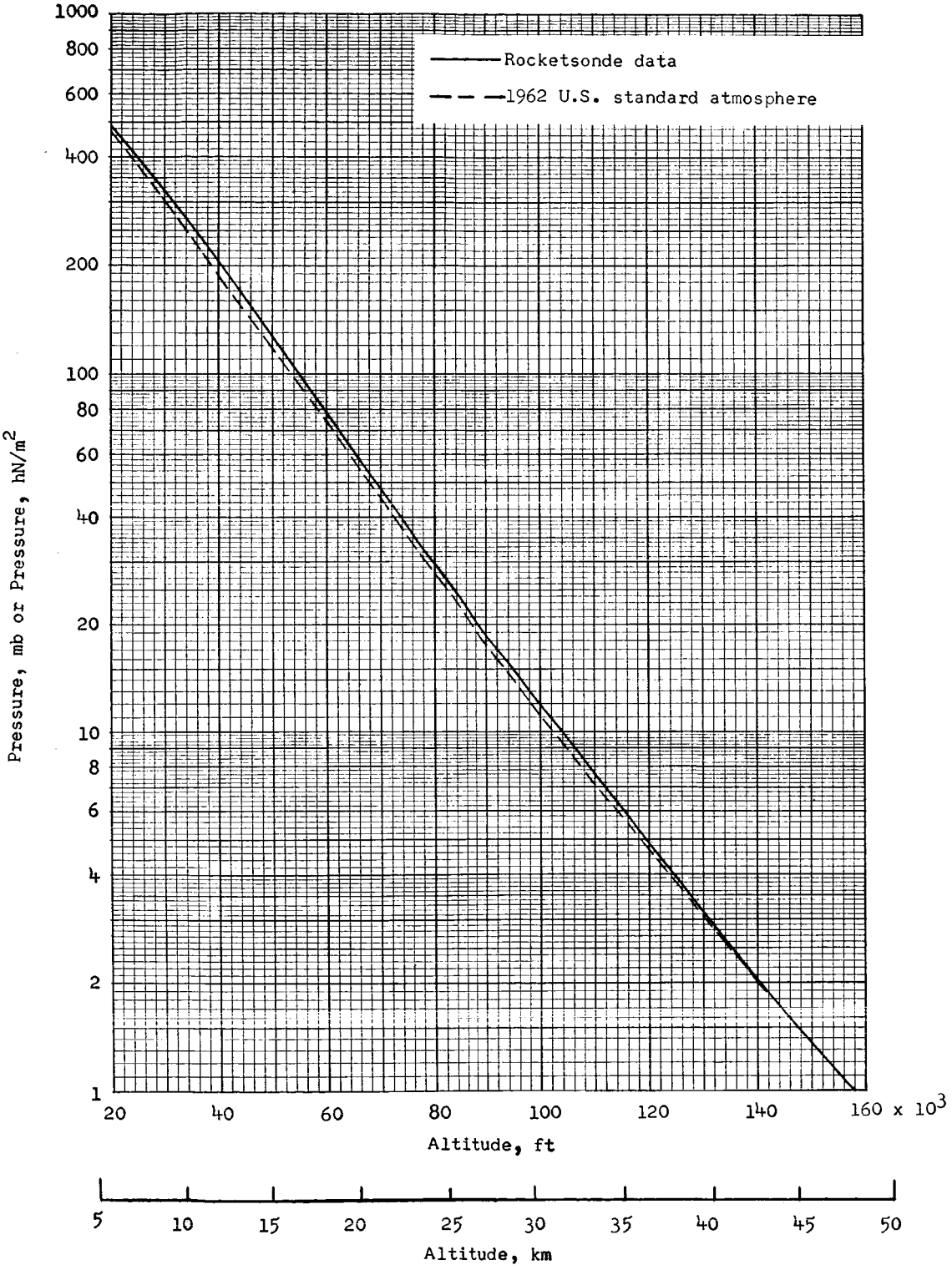

Figure 7.- Atmospheric pressure.

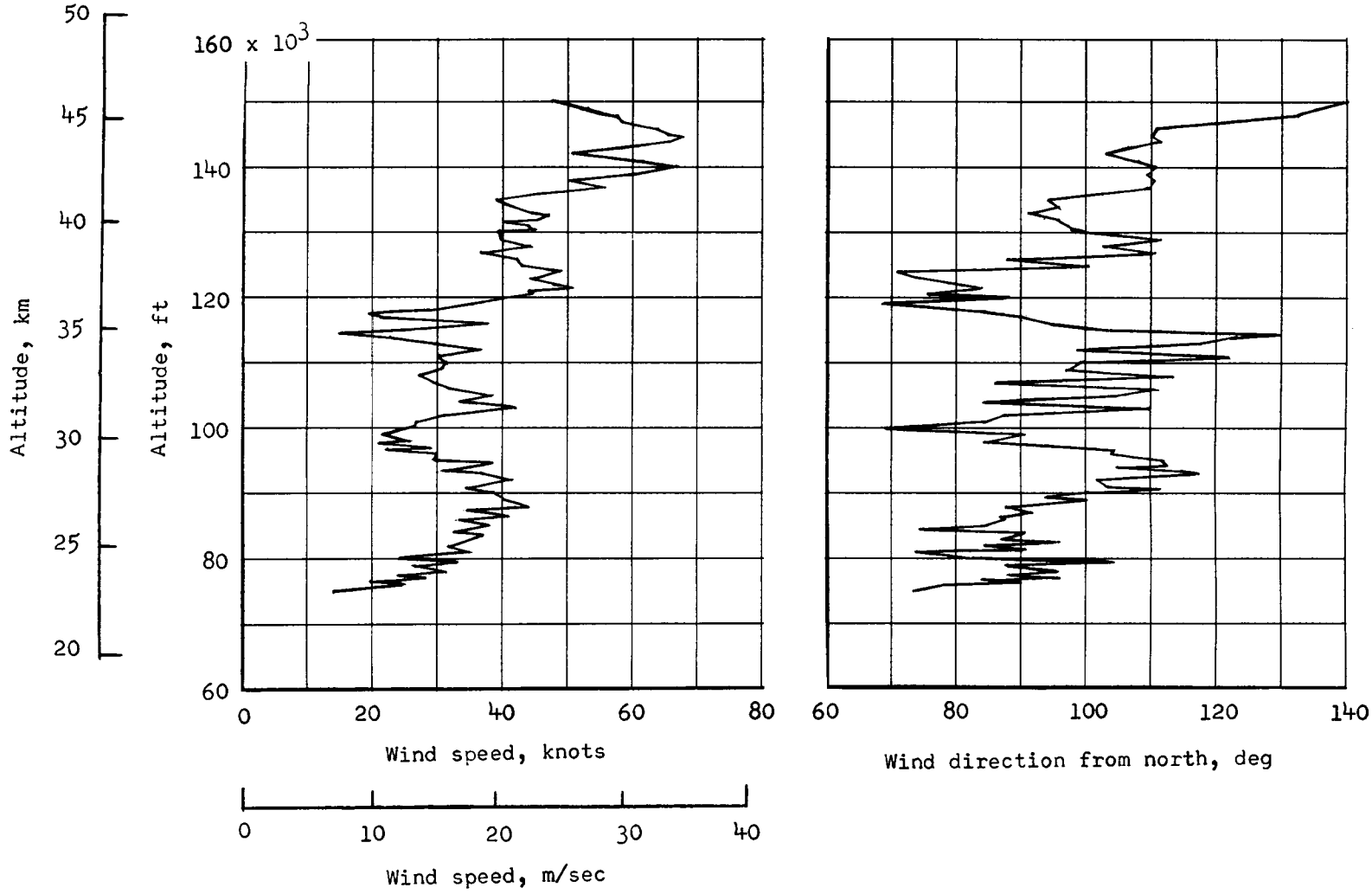

Figure 8.- Wind conditions.

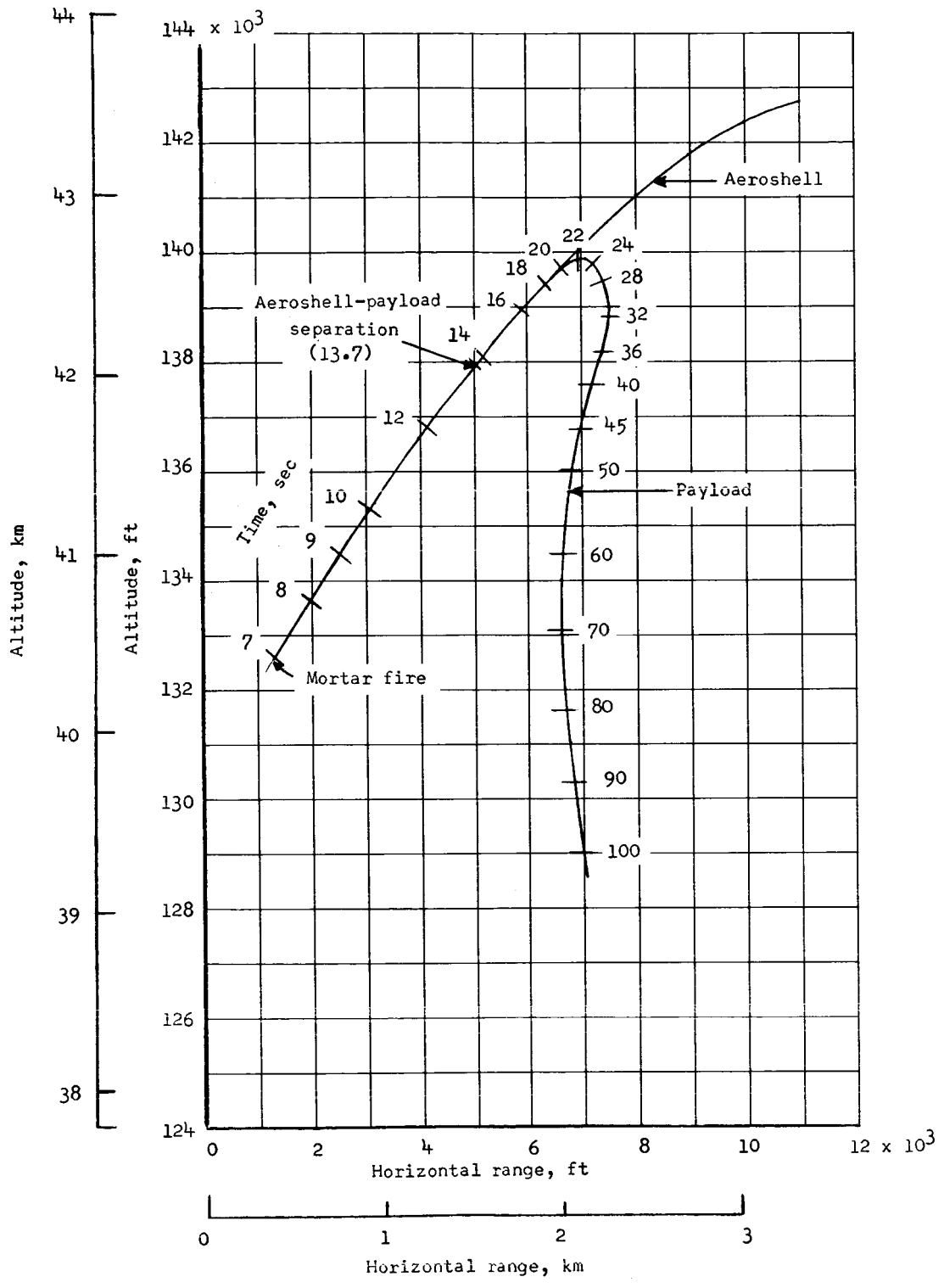

Figure 9.- Variation of altitude with horizontal range.

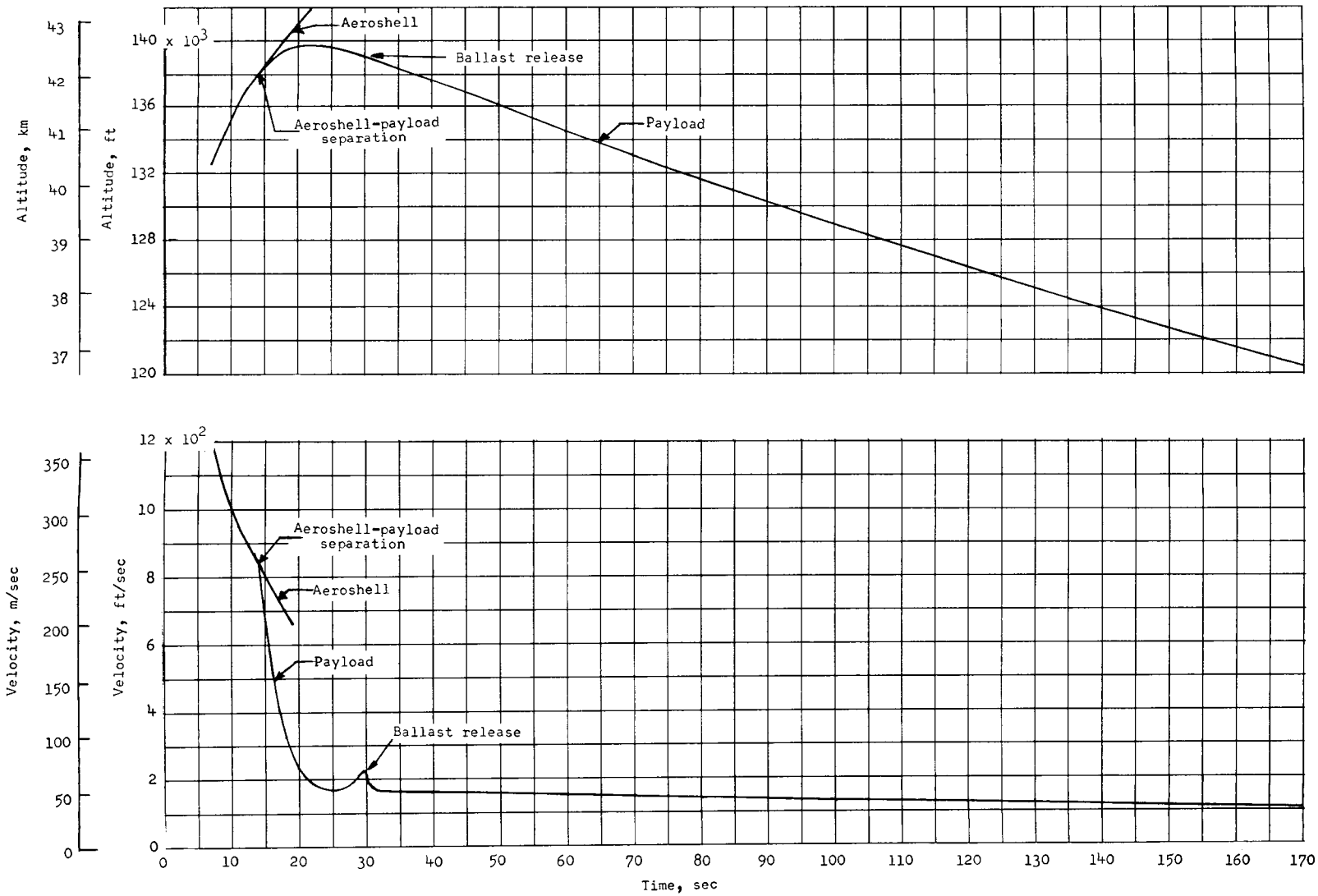

Figure 10.- Altitude and velocity time histories.

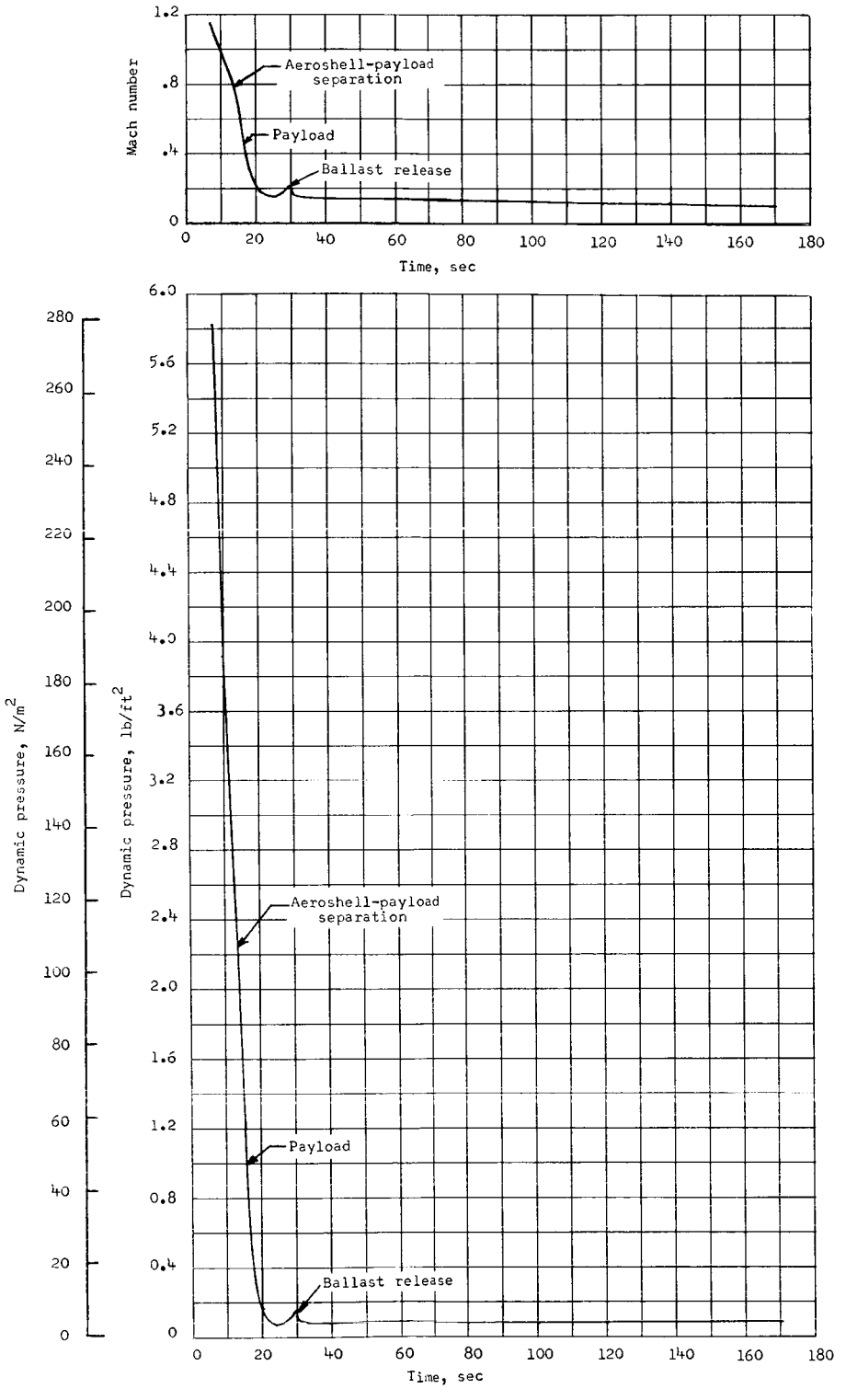

Figure 11.- Mach number and dynamic pressure time histories.

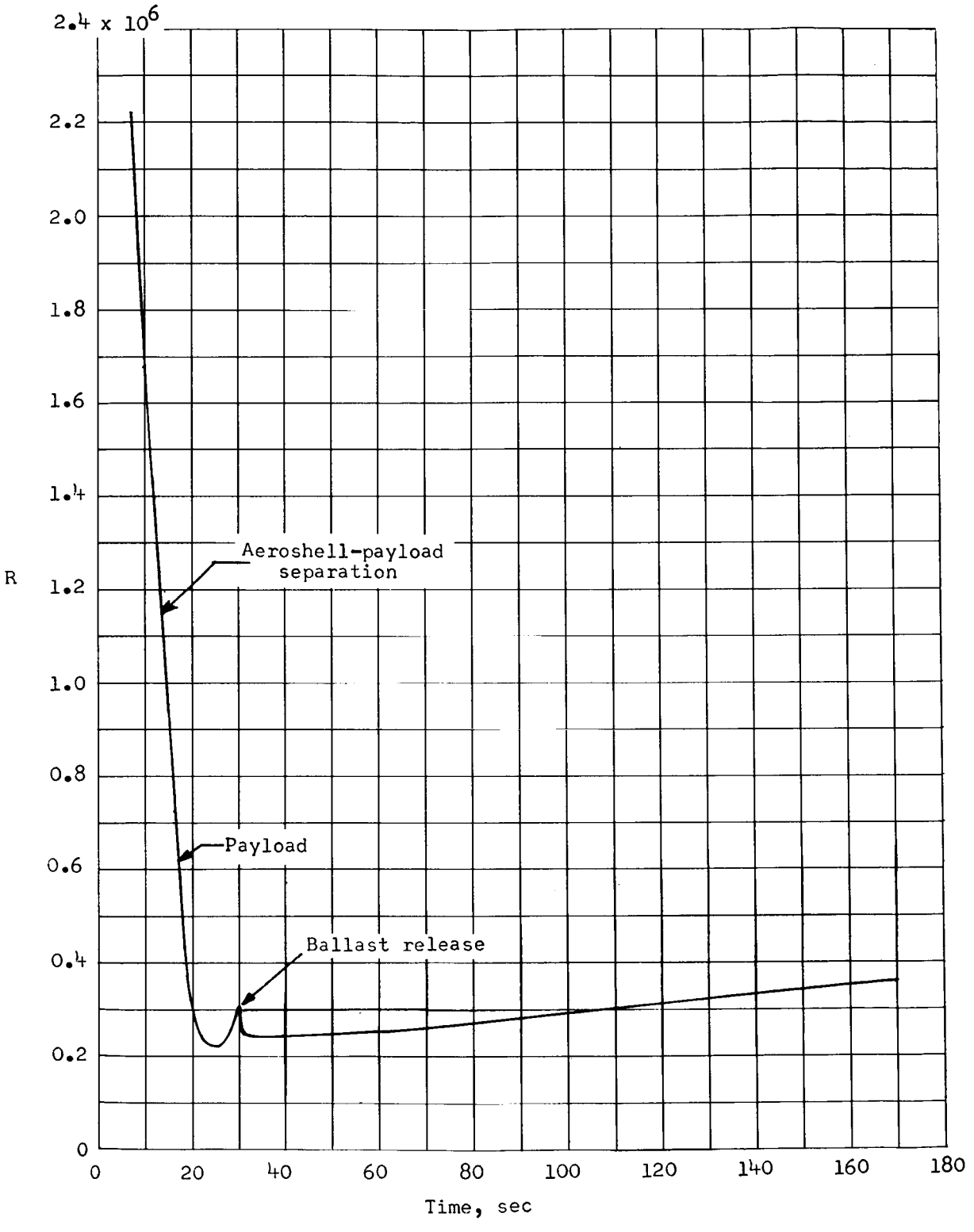

Figure 12.- Reynolds number time history (based on 85.3-foot nominal diameter).

Time = 7.87 seconds

Time = 8.16 seconds

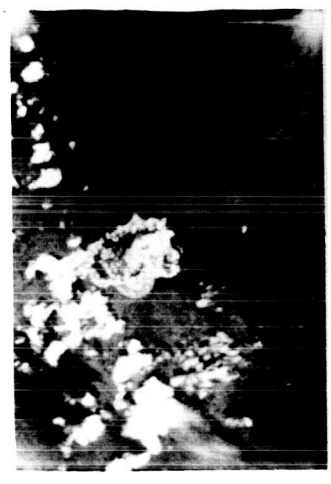

Time = 8.56 seconds

(a) Inflation to reefed condition. L-67-925

Figure 13.- Onboard camera photographs.

Time = 9.25 seconds

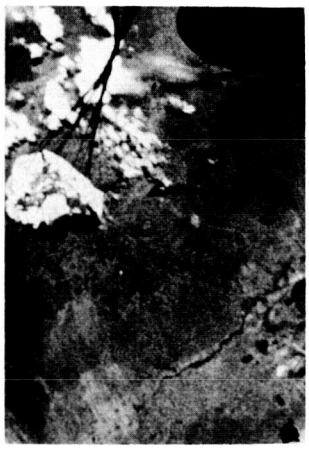

Time = 9.73 seconds

Time = 9.92 seconds

(b) Reefed condition. L-67-924

Figure 13.- Continued.

Time = 13.30 seconds

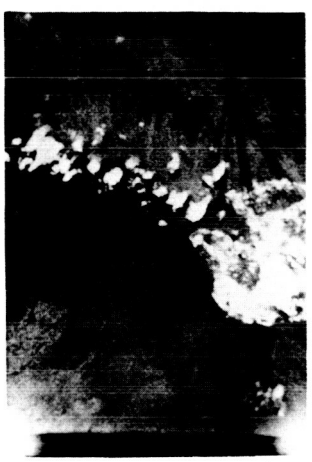

Time = 13.45 seconds

Time = 13.97 seconds

(c) Disreef to full-inflation condition. L-67-926

Figure 13.- Continued.

Time = 14.95 seconds

Time = 15.11 seconds

Time = 16.15 seconds

(d) Full-inflation condition. L-67-927

Figure 13.- Concluded.

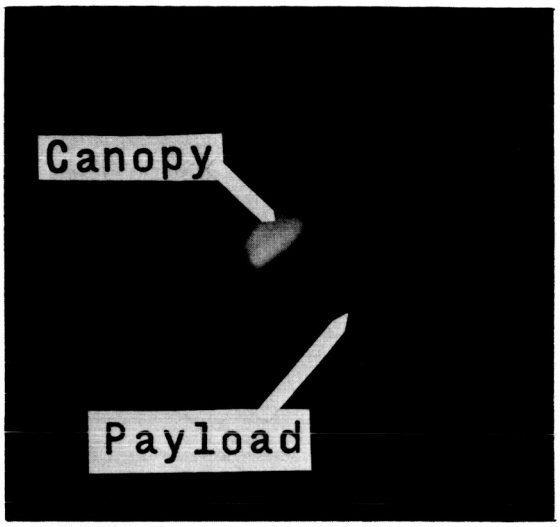

Apogee

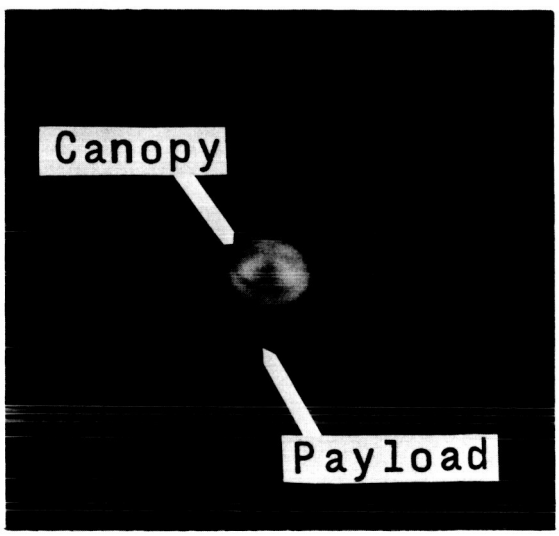

Descent

Figure 14.- Long-range ground camera photographs. L-67-923

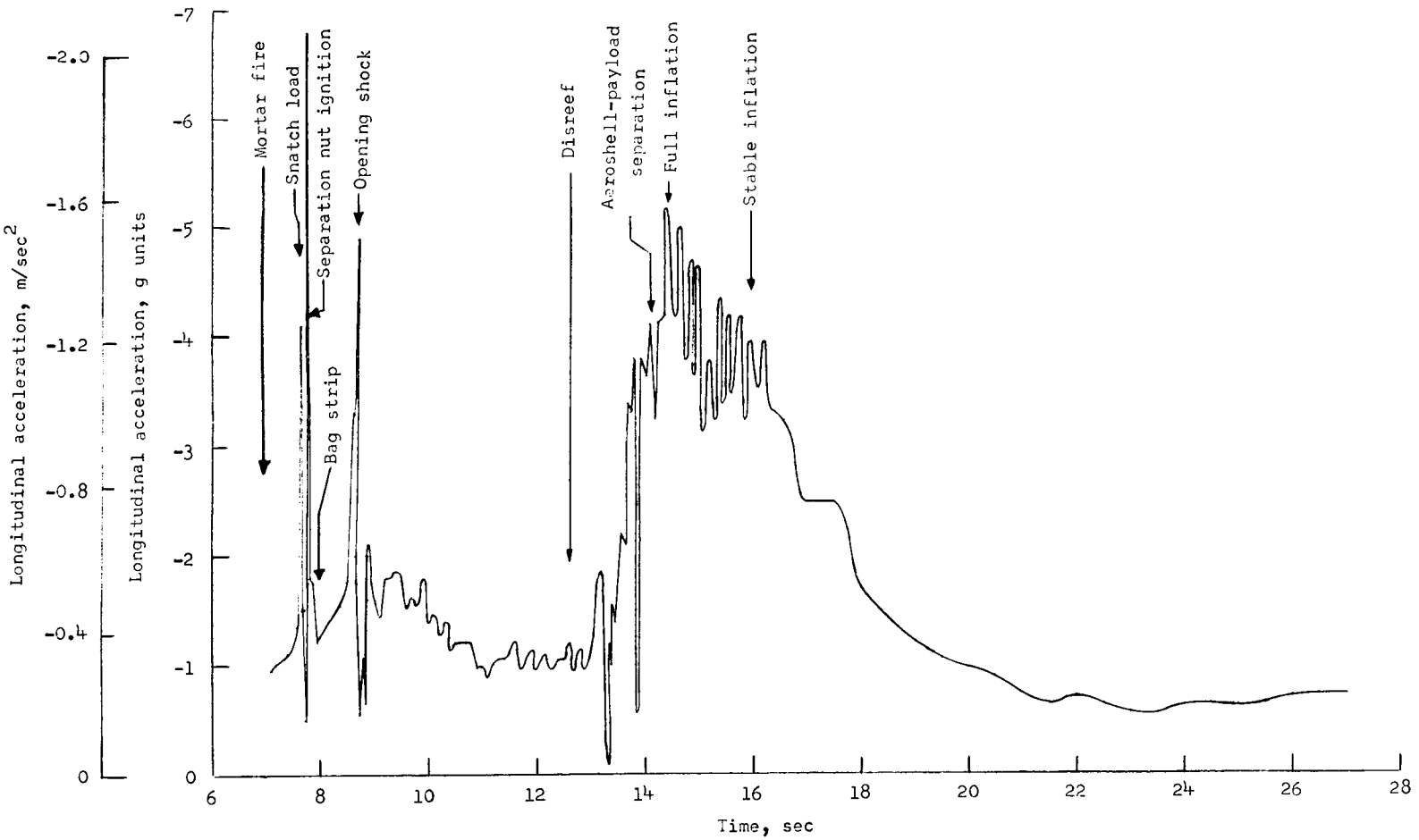

Figure 15.- Longitudinal acceleration time history.

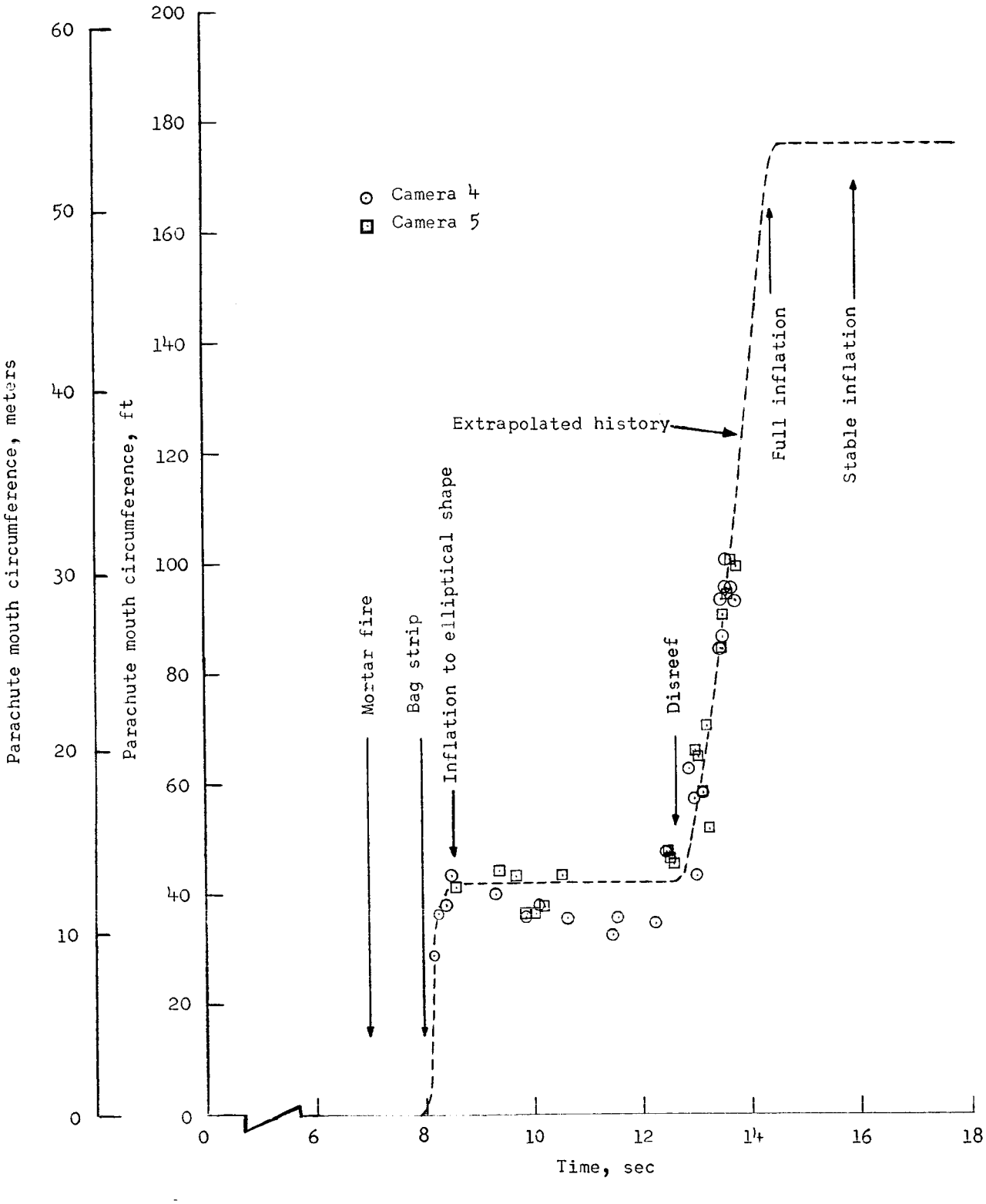

Figure 16.- Parachute mouth circumference time history.

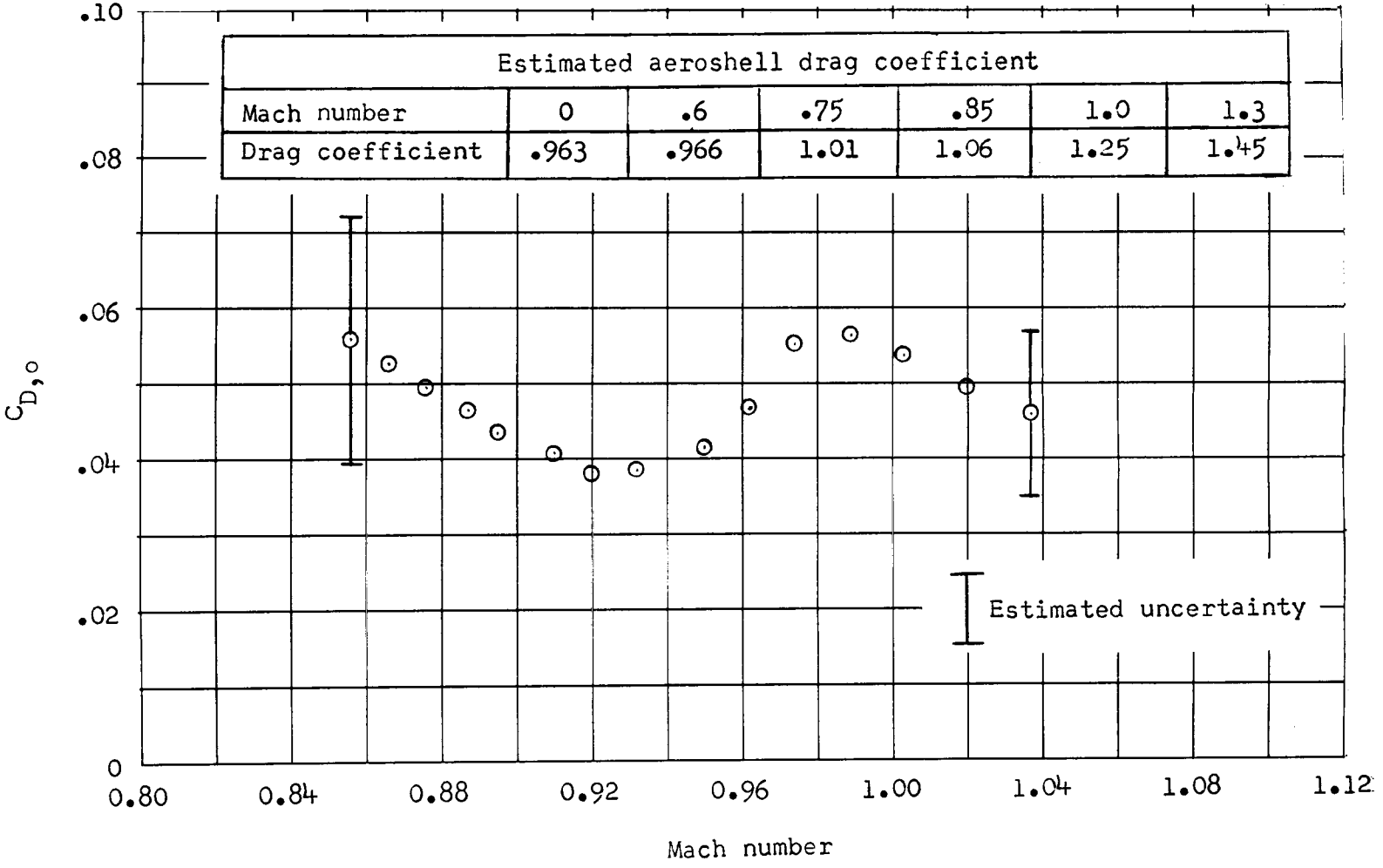

Figure 17.- Variation of drag coefficient with Mach number for reefed parachute (based on free-stream velocity and density and the nominal canopy area).

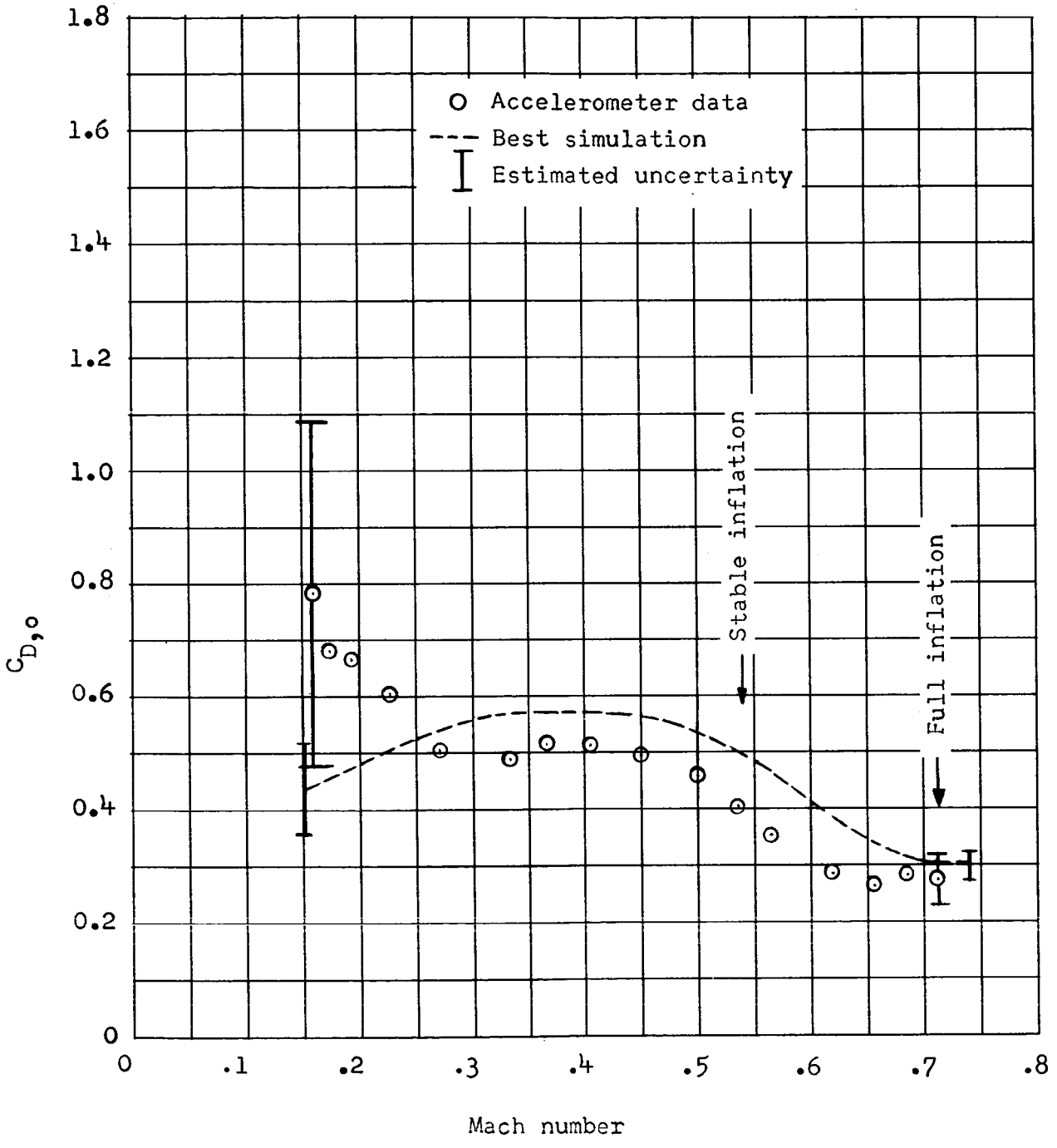

Figure 18.- Variation of drag coefficient with Mach number for full-inflation condition (based on nominal canopy area).

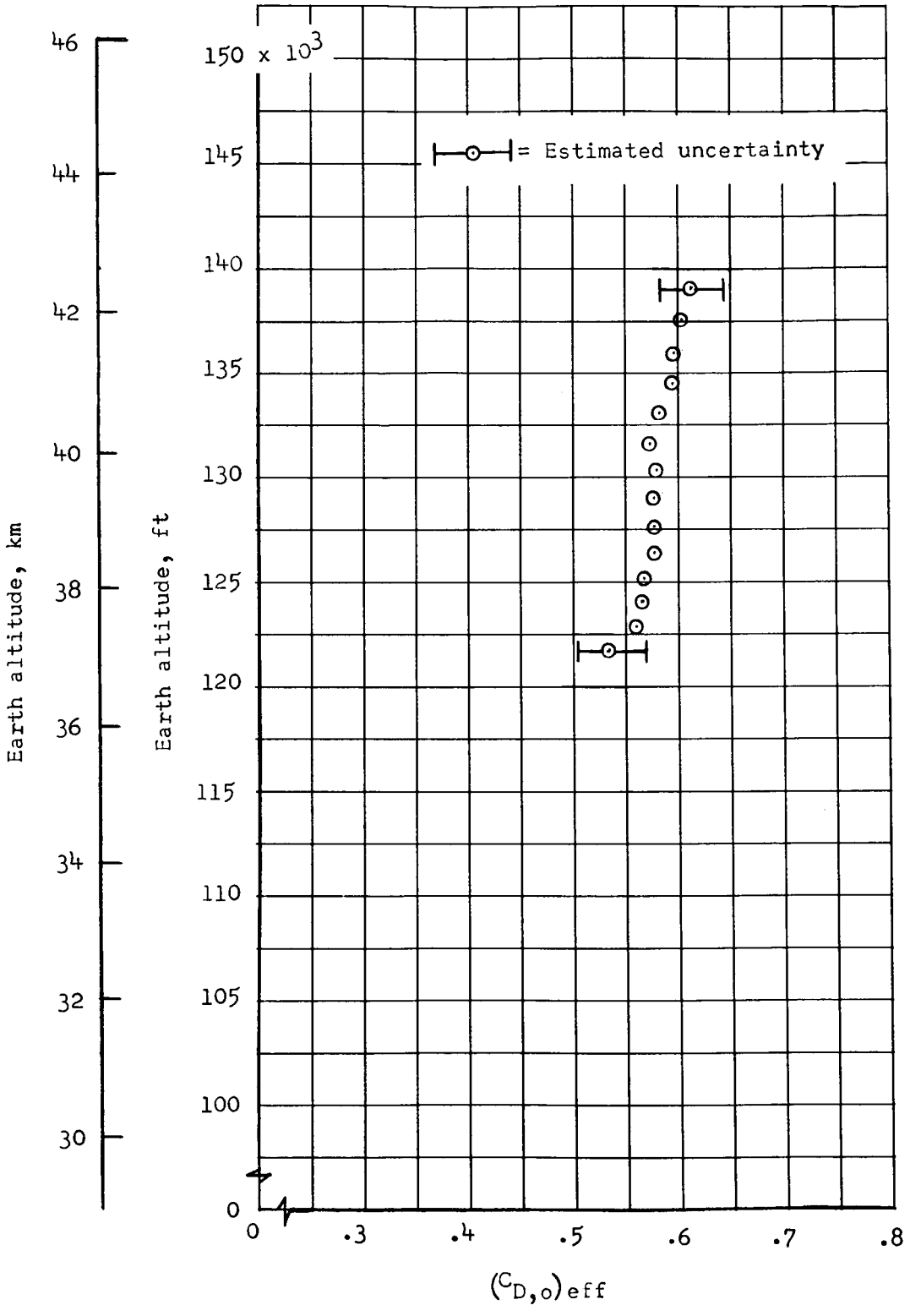

Figure 19.- Variation of altitude with effective drag coefficient.

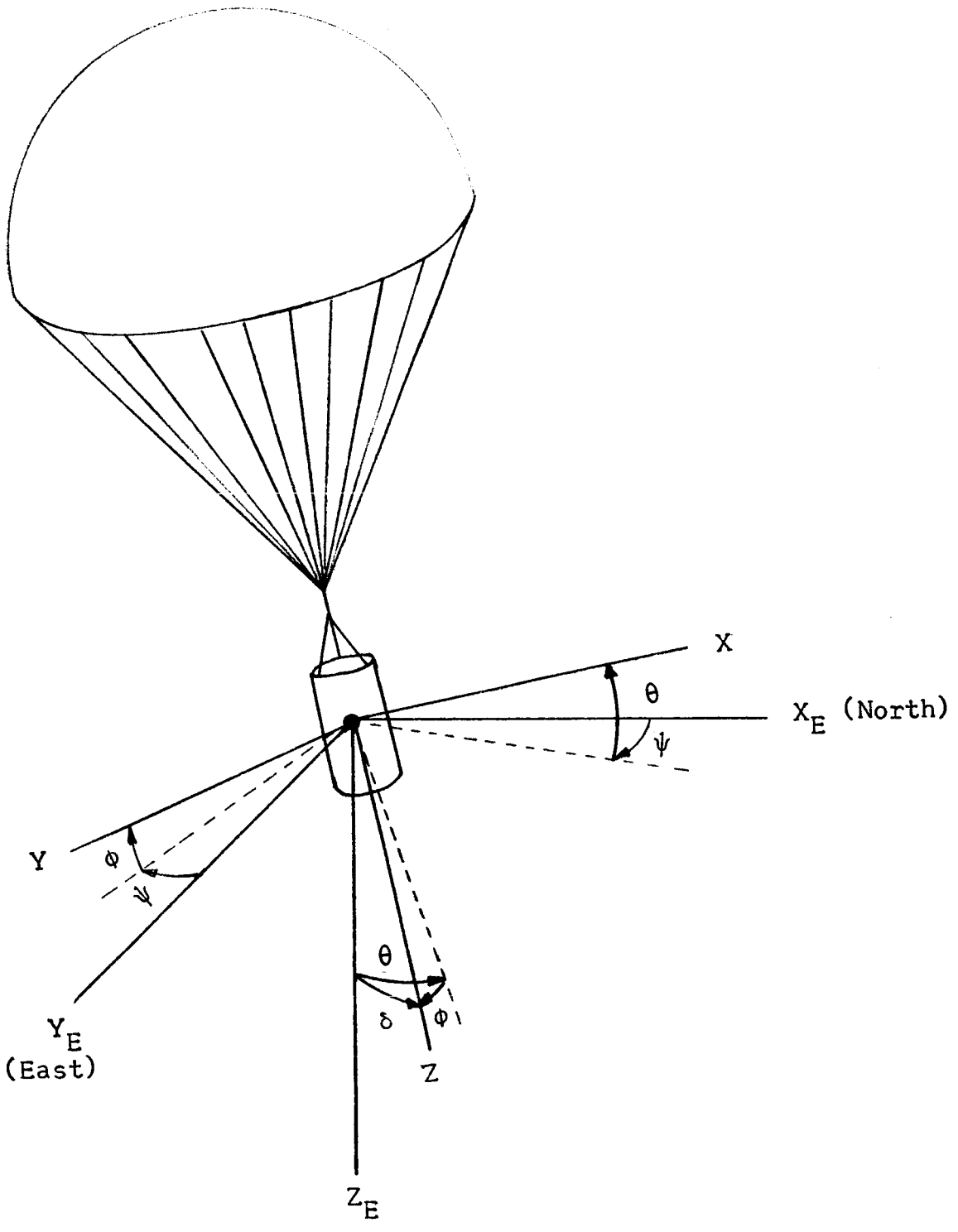

Figure 20.- Body-axis system orientation.

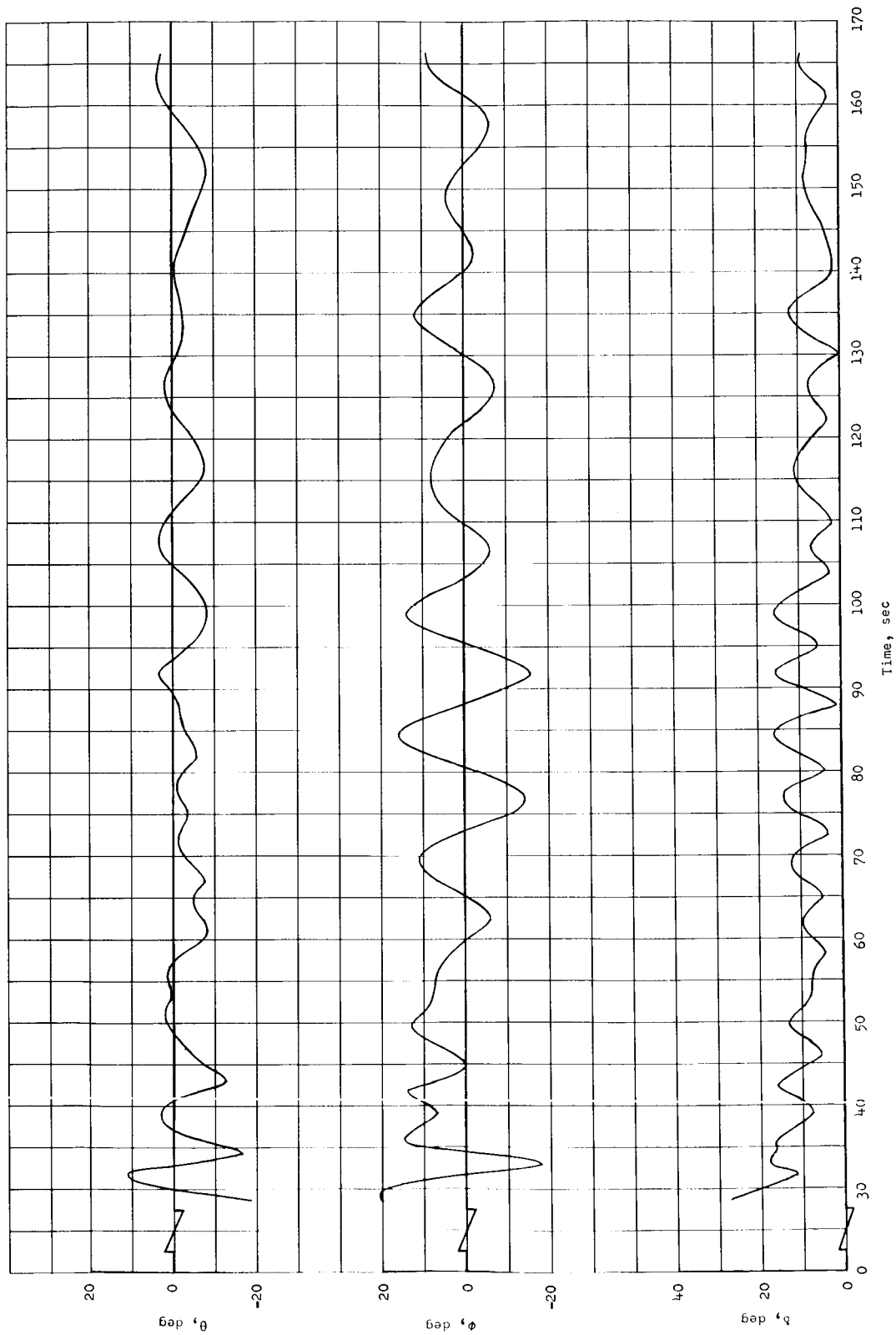

Figure 21.- Time histories of θ, Φ, and δ.

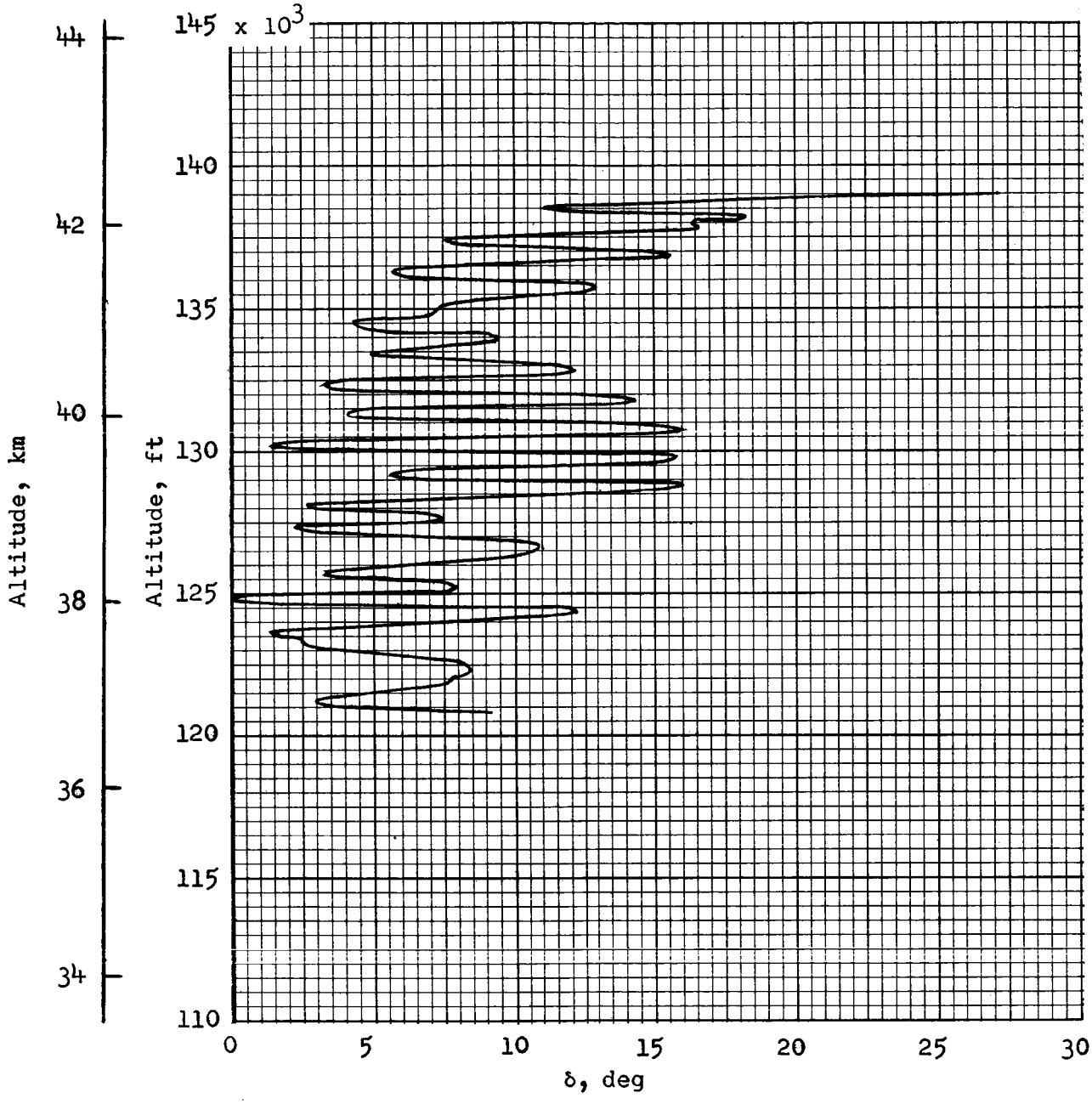

Figure 22.- Variation of altitude with δ.

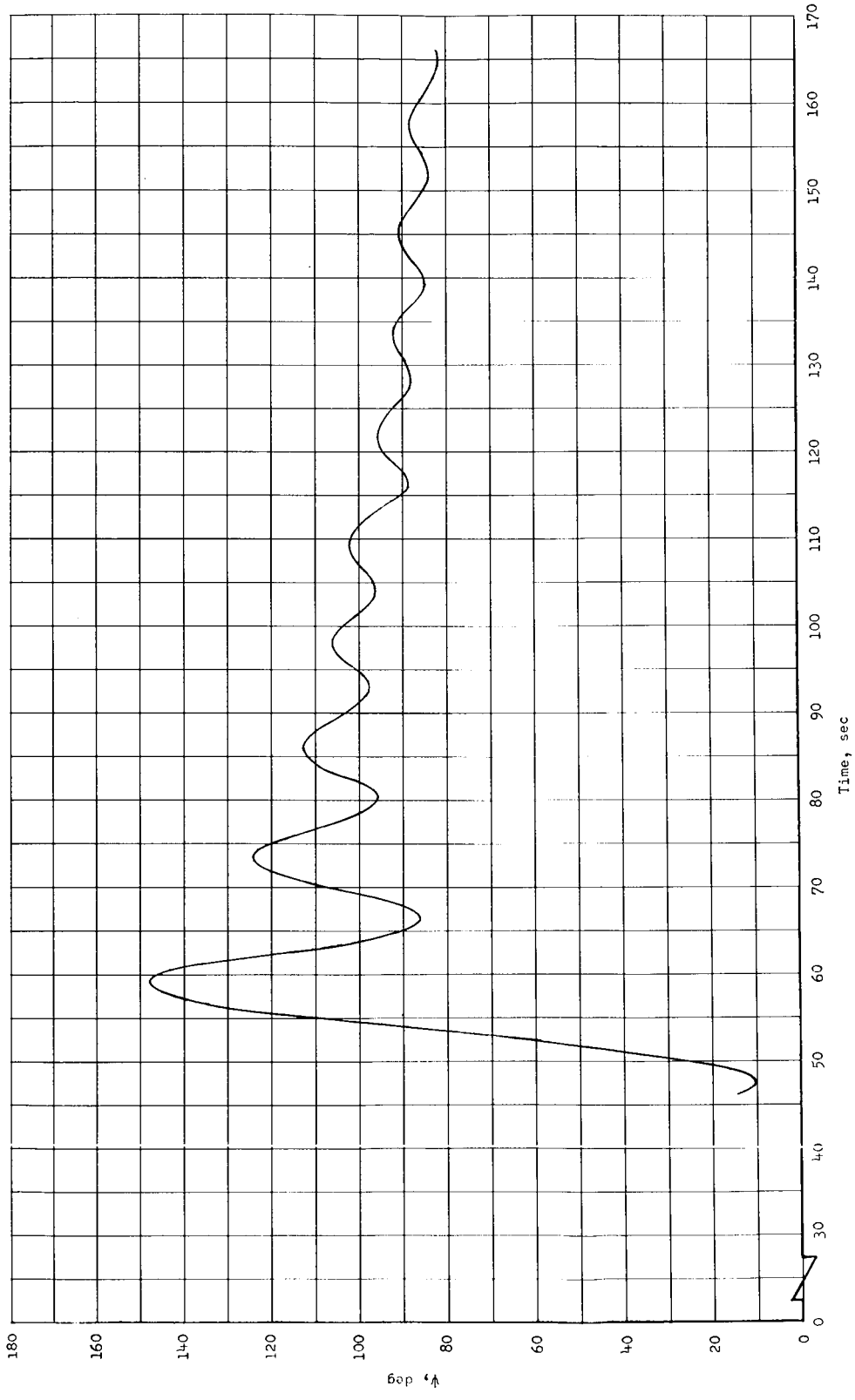

Figure 23.- Time history of ψ.